

Wind farm connected to a grid using fuzzy logic controller based the unified power flow controller

Rabyi Tarik, Brouri Adil

L2MC laboratory, SECNDCM teams, ENSAM, Moulay Ismail University, Meknes, Morocco

Article Info

Article history:

Received May 11, 2022

Revised My 30, 2022

Accepted Jun 13, 2022

Keywords:

Doubly-fed induction generator

Fuzzy logic controller

Power flow

Unified power flow controller

Wind farm

ABSTRACT

The doubly-fed induction generator (DFIG) based wind farm is widely used for extracting energy from the wind. When the wind farm is connected to the grid, generally it causes some perturbations. It can disturb the function of the grid and the installations connected to the grid. This impact concerns the load flow, voltage drops, and frequency fluctuations. To overcome those issues, the unified power flow controller (UPFC) is recommended. In this paper, we propose to study the impact of the integration of a wind farm on the power system. Presently, we propose an original contribution by using UPFC based on fuzzy logic controllers (FLC). Finally, simulation and experimental results using MATLAB/Simulink are proposed to show the effectiveness of this solution.

This is an open access article under the [CC BY-SA](https://creativecommons.org/licenses/by-sa/4.0/) license.



Corresponding Author:

Rabyi Tarik

L2MC laboratory, SECNDCM teams, ENSAM, Moulay Ismail University

Marjane 2, BP 15290, Al-Mansour ENSAM, 50000 Meknes, Morocco

Email: tarikensam@yahoo.fr

1. INTRODUCTION

Generally, renewable energy participates by an important percentage in the grid's global electricity production [1]. The wind power industry is one of the renewable energies that is undergoing rapid globalization. This power supply has been widely used in the last decades [2]. It has immense potential across the world and it can significantly reduce the dependence on fossil fuels [3]. The doubly-fed induction generator (DFIG) is one of the machines that are widely used in the wind power industry. Indeed, the DFIG presents many advantages compared to other machines. Specifically, it has a low cost. It can operate under variable wind speeds. The active and reactive powers of the DFIG can be easily controlled [4]. Many researchers had proposed several solutions to improve the dynamic performances of the DFIG and ameliorate the stability performances of the grid system. Wadawa *et al.* [5] propose an approach for hybrid control based on fuzzy logic, H infinity, and integral proportional controllers to supervise the speed of wind turbines (DFIG) connected to the electrical grid. Shabani *et al.* [6] propose the effect of the closed-loop control system with a generic PI is used to control the DFIG. The aim is to study the stability of the power system under the penetration of the DFIG-based wind farms. Tamalouzt *et al.* [7], a method based on the three-level inverter topology and using a direct reactive power control is proposed for a (DFIG)-based wind power plant system. Sahri *et al.* [8] introduce a direct power control strategy based on machine learning to overcome the difficulties caused by the DFIG and local reactive power variations from the grid.

The three main causes of perturbations that create harmonics and oscillations in the power grid are the integration of wind energy, the sudden insertion (increase or decrease) of the load, and the environmental causes. These problems can affect the system's stability and may lead to failure. To overcome these disturbances and ameliorate the power quality [9], flexible alternating current transmission system (FACTS)

devices are often used [10], [11]. The FACTS can be introduced in the power system network to increase the power transfer capability of the transmission line and to ameliorate the voltage stability [12], [13]. Then, the transient stability, voltage regulation, reliability, and thermal limits of the transmission network can be improved using the FACTS systems [12]. According to the connection type of the FACTS devices with the power system network, the compensation techniques can be classified into four types: series-connected controllers, shunt connected controllers, combined series-series controllers, and combined shunt-series controllers. The most used FACTS devices for series compensators are: thyristor-controlled series capacitor (TCSC), thyristor-controlled series reactor (TCSR), thyristor switched series capacitor (TSSC), and static synchronous series compensator (SSSC) [14]. The most used FACTS devices for shunt compensators are: static VAR compensator (SVC) [15], thyristor-controlled reactor (TCR), thyristor switched capacitor (TSC) [16], thyristor switched reactor (TSR), and static synchronous compensator (STATCOM) [17]-[19]. The most used FACTS devices for series-series compensators are the interline power flow controllers (IPFC). The main FACTS devices in the series-shunt compensator are the unified power flow controller (UPFC) [20], [21].

Liu *et al.* [22] discuss the global and local power flow operations conditions of the UPFC. A solution based on the wavelet-alienation-neural technique has been established and studied for the fault analysis of a grid operating with UPFC in [23]. Hinda *et al.* [24], an advanced control scheme based on sliding mode control of a UPFC was introduced.

Kotb *et al.* [25] introduce a fuzzy logic controllers (FLC) method supervising the exchange of energy in a microgrid. The aim is to improve the stability and power quality of the microgrid. In [26], an adaptive fuzzy controller was implemented using only the output signals. Then, the path of the mechatronic system can be accurately determined. Ghosh [27], a neuro-fuzzy-based on the internet of things is proposed. This work aims to reduce the production cost of the power system. To optimize the wind power system, an adaptive fuzzy logic controller (AFLC) has been suggested in [28]. This AFLC was presented as a regulator for extracting the peak power from a permanent magnet synchronous generator-based wind turbine. In [29], a fuzzy PID combined with a genetic algorithm is designed to control the charger of the auxiliary power supply of a train. To transfer the active power generated to the grid system with a unity power factor, a FLC of active and reactive power for a grid-connected photovoltaic system was applied in [30].

Accordingly, the integration of a DFIG-based wind farm into the power system has an influence on the load flow, the voltage drops, and the frequency fluctuation. To overcome these impacts and to ameliorate the dynamic performances of this integration, the UPFC system can be implemented in the grid. However, several previous works have proposed the integration of the wind farm into the grid. To overcome the problems of disturbances and to ameliorate the power quality, the FACTS devices have been proposed. In this work, an approach based on fuzzy logic control is established to control the UPFC. Then, this strategy is different from other techniques. It is based on three FLC that have been implemented in the UPFC. Then, two power plants connected to the grid are studied. This constitutes one of the main novelties of this work. Summary of main contributions, the main contributions of this paper can be summarized as:

- Presently, the integration of wind farms into the grid is proposed.
- A solution using the UPFC is studied to overcome the disturbance problems caused by this integration.
- To enhance the power supply quality, a FLC is proposed to control the UPFC. Specifically, in the UPFC-shunt two regulators (based on the FLC) are introduced. The first one is designed to control the AC voltage part and the second is intended to supervise the DC voltage regulator.
- Furthermore, a power regulator based on the FLC is implemented in the UPFC series.
- It is shown that the proposed solution using the UPFC based on the FLC can improve the system characteristics.
- It is noticed that the suggested algorithm is featured by a high convergence rate to achieve the global optima.

The remaining sections of this paper will be organized as follows: the mathematical model of the DFIG is introduced in section 2. The UPFC is dealt with in section 3. The FLC-based UPFC is presented in section 4. The different cases of the system under study are described in section 5. Simulation results and comparisons are also given in this section. In section 6, the key points of this paper are summarized as a conclusion.

2. DFIG MODELING

The model of the studied DFIG connected to the electrical grid is given in Figure 1. By referencing to the dq Park reference, the mathematical modeling of the voltages, and active/reactive powers of the DFIG is [8]:

- Voltage equations

$$V_{ds} = R_s i_{ds} + \frac{d\phi_{ds}}{dt} - w_s \phi_{qs} \tag{1}$$

$$V_{qs} = R_s i_{qs} + \frac{d\phi_{qs}}{dt} + w_s \phi_{ds} \tag{2}$$

$$V_{dr} = R_r i_{dr} + \frac{d\phi_{dr}}{dt} - (w_s - w_r) \phi_{qr} \tag{3}$$

$$V_{qr} = R_r i_{qr} + \frac{d\phi_{qr}}{dt} + (w_s - w_r) \phi_{dr} \tag{4}$$

where (ϕ_s, ϕ_r) , (V_s, V_r) , (i_s, i_r) , (w_s, w_r) and (R_s, R_r) are the flux, voltage, current, pulsations, and resistances of the stator and rotor respectively.

– Power equations

$$P_s = \frac{3}{2} (V_{ds} i_{ds} + V_{qs} i_{qs}) \tag{5}$$

$$Q_s = \frac{3}{2} (V_{qs} i_{ds} - V_{ds} i_{qs}) \tag{6}$$

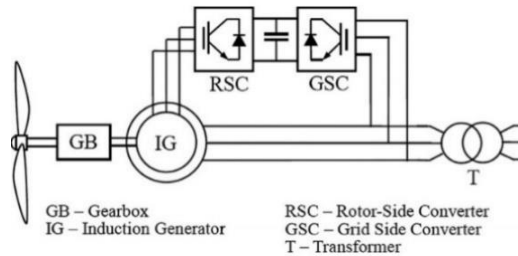


Figure 1. DFIG-based wind farm connected to the grid

3. BASIC STRUCTURE OF UPFC

To satisfy the electrical market, the electrical equipment should respect the requirements of network characteristics. Therefore, the use of FACTS devices can be an important solution [31]. The FACTS devices are combinations of power electronics and traditional power system components. These devices can improve transient and dynamic stability, voltage regulation, and power system reliability [32]. Among the FACTS devices, the UPFC is the most important one. Indeed, this latter can control the active and reactive power flows in the electrical transmission line. The UPFC is constituted by shunt voltage-source converter (VSC), which works as a static compensator (STATCOM), and series VSC, which works as a static synchronous series compensator (SSSC). The STATCOM and the SSSC are coupled by a common DC link as shown in Figure 2.

The UPFC can be considered as a multi-function controller which combined the performance of two FACTS devices. The single-phase representation of the three-phase UPFC system is shown in Figure 3. The current through the series and shunt branch of the circuit in Figure 3 can be expressed by (7) and (8).

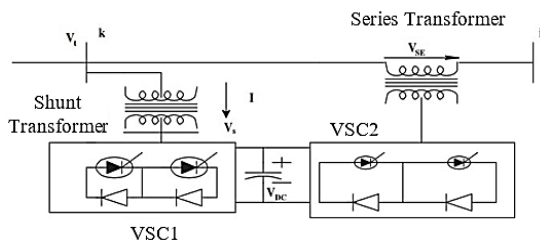


Figure 1. UPFC single line diagram

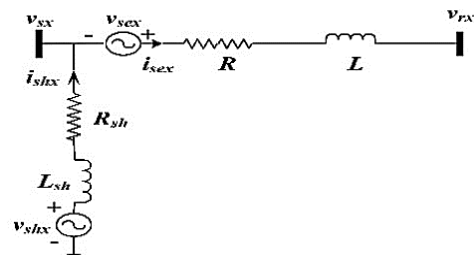


Figure 2. Single-phase representation of three-phase UPFC system

$$L \frac{di_{sex}}{dt} = -Ri_{sex} + v_{sex} + v_{sx} - v_{rx} \tag{7}$$

$$L \frac{di_{shx}}{dt} = -Ri_{shx} + v_{shx} - v_{sx} \tag{8}$$

Where (v_{sex}, v_{shx}) , (R, R_{sh}) and (L, L_{sh}) are voltage sources, resistance, and leakage inductance of the series and shunt converters of the UPFC respectively. The ‘x’ represents the three-phase quantities (phase a, b or c).

4. FUZZY LOGIC CONTROLLER BASED UPFC

To improve the power quality after integration of the wind energy in the grid, a solution using UPFC based on a fuzzy logic controller is proposed. The UPFC is composed of shunt and series controllers. The shunt controller of UPFC is constituted by 3 regulators. Specifically, the current, the DC voltage, and the AC voltage regulators. Each regulator has a PI controller. In the series controller of UPFC, there are also two PI controllers implemented in the power regulator. Generally, a PI controller presents many advantages. This controller combines the benefits of the P and I regulators. The PI controller gives good performances with simple implementations and structures. However, the PI controller has often some limitations in nonlinear systems. To improve the UPFC performances, we propose solutions combining a FLC with the PI controllers. The structures of these regulators are shown in Figure 4, Figure 5, and Figure 6.

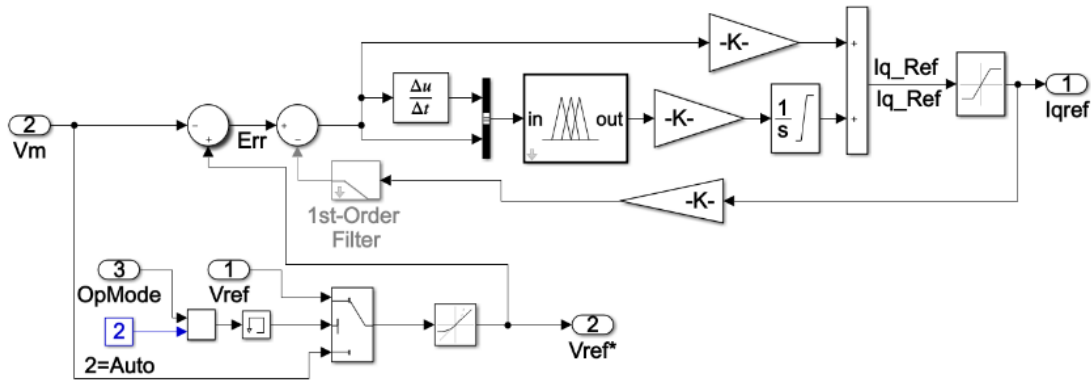


Figure 3. The AC voltage regulator, based on the FLC, in the UPFC shunt

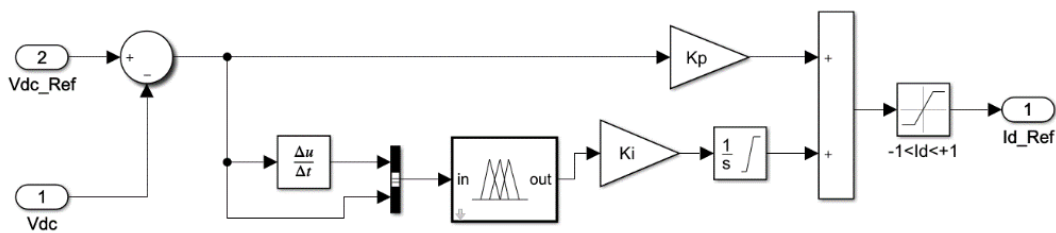


Figure 4. The DC voltage regulator, based on the FLC, in the UPFC shunt

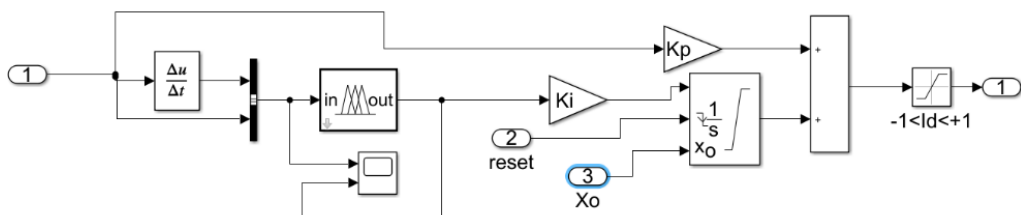


Figure 5. The power regulator in the UPFC series based on the FLC

Note that the FLC has been widely used in several applications compared to other control strategies. The integration of the FLC can present several advantages, e.g., in nonlinear systems. Generally, the most used FLC types are Mamdani and Takagi-Sugeno. Presently, the FLC based on the Mamdani-type is proposed. The integral part of the PI is adjusted by the FLC while the proportional term is kept unchanged. The main components of the FLC are fuzzification blocks, fuzzy rule bases, and defuzzification blocks. The proposed fuzzy control module contains two inputs (the error ε and the derivative of the error $\dot{\varepsilon}$) and one output, noted α_j ($j = 1,2,3$). In this work, the chosen basic universes of input and output parameters are $[-1,1]$, i.e., $\varepsilon, \dot{\varepsilon} \in [-1,1]$ and $\alpha_1, \alpha_2, \alpha_3 \in [-0.01,0.01]$. We assign seven fuzzy sets for the inputs and output, namely {negative big (NB), negative middle (NM), negative small (NS), zero (ZZ), positive small (PS), positive middle (PM), positive big (PB)}. In this paper, the membership functions linked to $\varepsilon, \dot{\varepsilon}$, and α_j are of triangular shapes. For simplification reasons, we will choose the same fuzzy subsets for the input variables and the same fuzzy subsets for the output variables. The membership functions for the input and output are shown in Figure 7 and Figure 8, respectively.

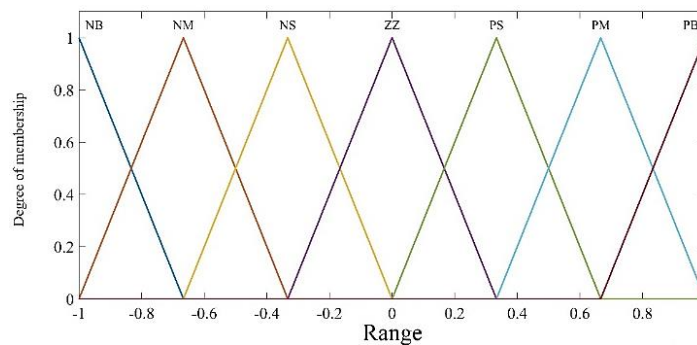


Figure 6. Membership functions of inputs $\varepsilon, \dot{\varepsilon}$

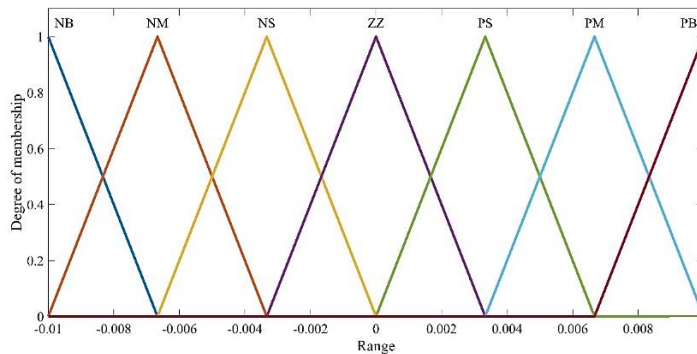


Figure 7. Membership functions of output variables

5. SIMULATIONS AND DISCUSSION

5.1. Simulation of five nodes grid and system connected with DFIG-based wind farm

A standard load flow study is based on the determination of voltage magnitude, phase angle, active and reactive in the buses. Generally, there are three types of buses: load bus, PV bus, and slack bus. In the load bus (known as PQ bus), the real and reactive powers are already determined and there is no production of energy. The voltage and real power produced by the PV bus (known as generator bus) are constant. The active and reactive power in the grid can be adjusted by the slack bus (known as the reference bus or swing bus).

The aim presently is to study the main five nodes in the grid based on the Newton Raphson method [33]. This method is based on the determination of the voltage magnitude and the angle corresponding to each bus in the power system. Therefore, the active and reactive powers can be determined. The system under study is shown in Figure 9 and is composed of:

- Five buses (1 to 5) interconnected through three transmission lines ($L1 = 65\text{ km}$, $L2 = 50\text{ km}$, and $L3 = 50\text{ km}$)
- Two power plants providing 2200 MW. The first power plant is considered a slack bus providing the nominal power of 1200 MW. The second power plant is considered a PV bus which provides 1000 MW. The plant models include a power system stabilizer (PSS), an excitation system, and a speed regulator.
- Two transformer banks Tr1 and Tr2 characterized by 60 kV/220 kV.
- The load bus is characterized by an active power of 500 MW and a reactive power of 20 MVAR.

The integration of a wind farm into the power system can cause many disturbances. To study the disturbances caused by this integration, two simulations are proposed. In simulation 1 (Figure 9), there are two power plants. In simulation 2 (Figure 10), one of the power plants is replaced by a wind farm and it is considered as a power generator (PV bus) of 9 MW.

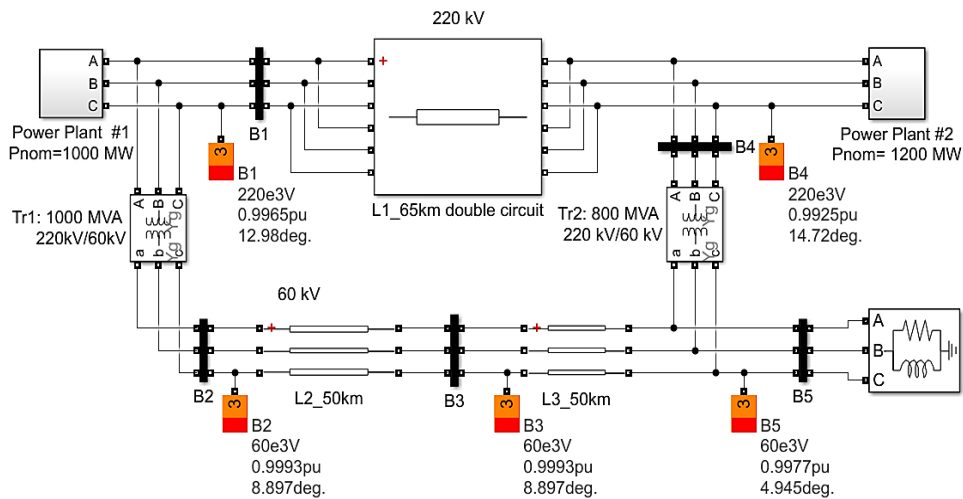


Figure 8. The grid schema with two power plants

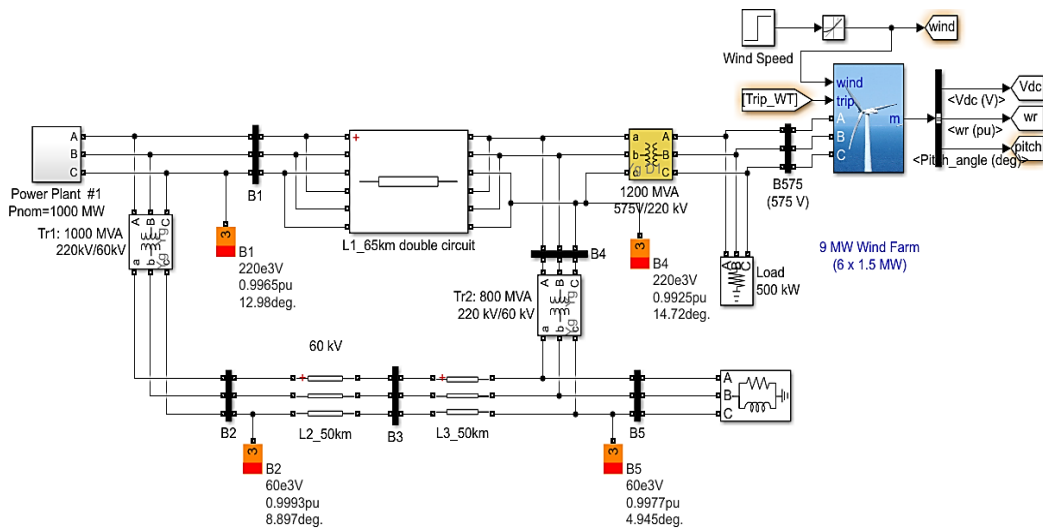


Figure 9. DFIG-based wind farm connected to the system

The curves of the voltage magnitude (V_{pos}) corresponding to each bus are illustrated in Figure 11 and Figure 12. By comparing these results, it is noticed that, when the UPFC is not introduced, a significant voltage drop is observed in bus 5. To show also the impact of the integration of the wind farm before and after integration, the curves of active (Figure 13 and Figure 14) and reactive powers (Figure 15 and Figure 16) are plotted respectively. Upon the start of the wind farm, this latter absorbs the active and reactive powers. This remark is confirmed by comparing the results given in Figure 14 and Figure 16 with those shown in Figure 13 and Figure 15, respectively.

The simulation results of the voltage magnitude, real power, reactive power, and phase angle corresponding to buses 1 to 5 are summarized in Table 1. For simulation 1, these results show that the obtained voltage in each bus varies between 0.97 *PU* and 0.98 *PU*. In the 5th bus, denoted load bus, the real and reactive powers converge respectively to: $P = 495.2 \text{ MW}$ and $Q = 19.81 \text{ MVAR}$. By comparing these values to the requirements of the load (500 *MW*, 20 *MVAR*), it is seen that this load can be satisfied.

Furthermore, by comparing the voltage values given in Table 1 and Table 2, it is shown that the voltage values are decreased in simulation 2. This confirms that the integration of the wind farm also disturbs the voltage. Finally, from the results obtained in the 5th bus (load node), we conclude that the load is now not satisfied, because we only obtain $P = 460.8 \text{ MW}$ (less than the required active power 500 *MW*) and $Q = 18.43 \text{ MVAR}$.

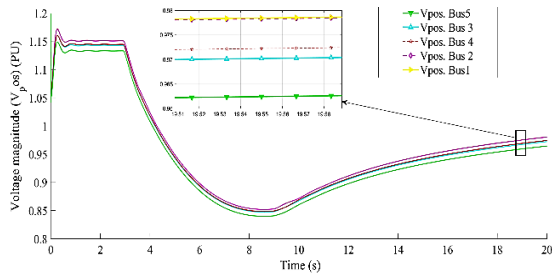


Figure 10. The curves of V_{pos} of each bus, obtained from simulation 1

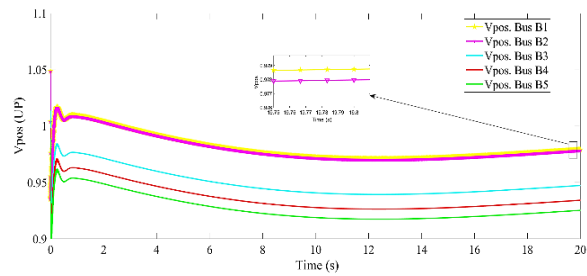


Figure 11. The curves of V_{pos} of each bus, obtained from simulation 2

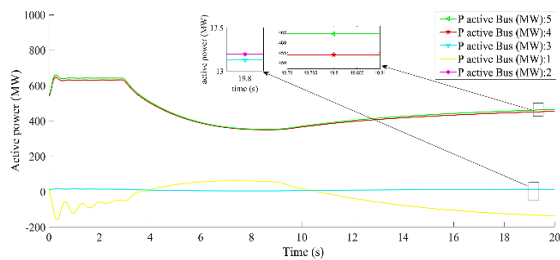


Figure 12. The curves of active powers obtained from simulation 1

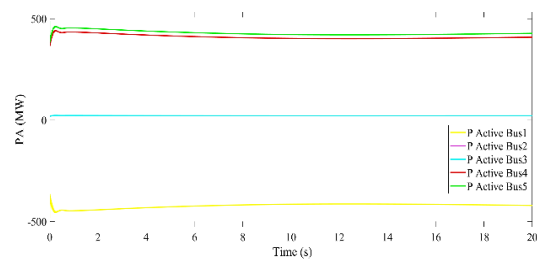


Figure 13. The curves of active powers obtained from simulation 2

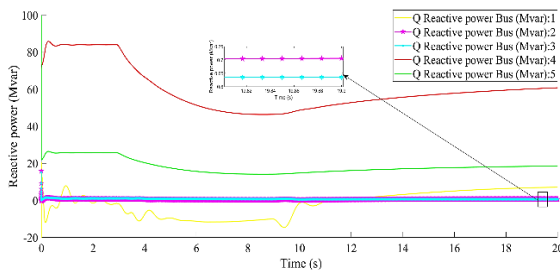


Figure 14. The curves of reactive powers obtained from simulation 1

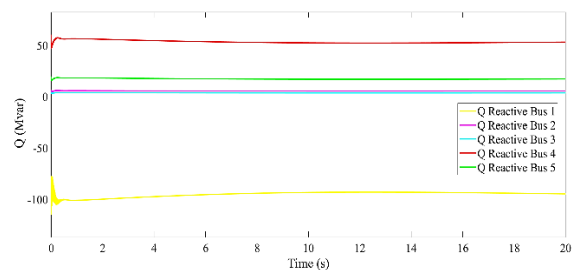


Figure 15. The curves of reactive powers obtained from simulation 2

Table 1. The obtained results from simulation 1 corresponding to each bus

Bus	B1	B2	B3	B4	B5
P (MW)	-159.1	6.769	6.753	496.4	495.2
Q(MVAR)	10.35	-0.37	0.23	36.01	19.81
V(PU)	0.98	0.98	0.98	0.98	0.97
d(°)	12.98	8.897	6.51	14.72	4.946

Table 2. The obtained results from simulation 2 corresponding to each bus

Bus	B1	B2	B3	B4	B5
P (MW)	-464.8	15.9	15.8	452.5	460.8
Q(MVAR)	-77.02	3.074	2.55	32	18.43
V(PU)	0.98	0.98	0.96	0.94	0.94
d(°)	12.98	8.897	6.51	14.72	4.946

5.2. System connected to DFIG-based wind farm and UPFC

To control the power flow and to avoid disturbances caused by the integration of the wind farm, examples of simulations using the UPFC are proposed (Figure 17). There are two simulations. In the first one (simulation 3), we used a UPFC. In the second one (simulation 4), we improved the control of the UPFC by implementing a FLC. The obtained results from simulations 3 and 4 corresponding to each bus are summarized in Table 3 and Table 4. In simulation 3, it is seen that the voltage value in the 3rd bus increased from 0.96 PU (Table 2) to 1.06 PU (Table 3). Also, the voltage in the 4th and 5th buses increased from 0.94 PU to 0.95 PU.

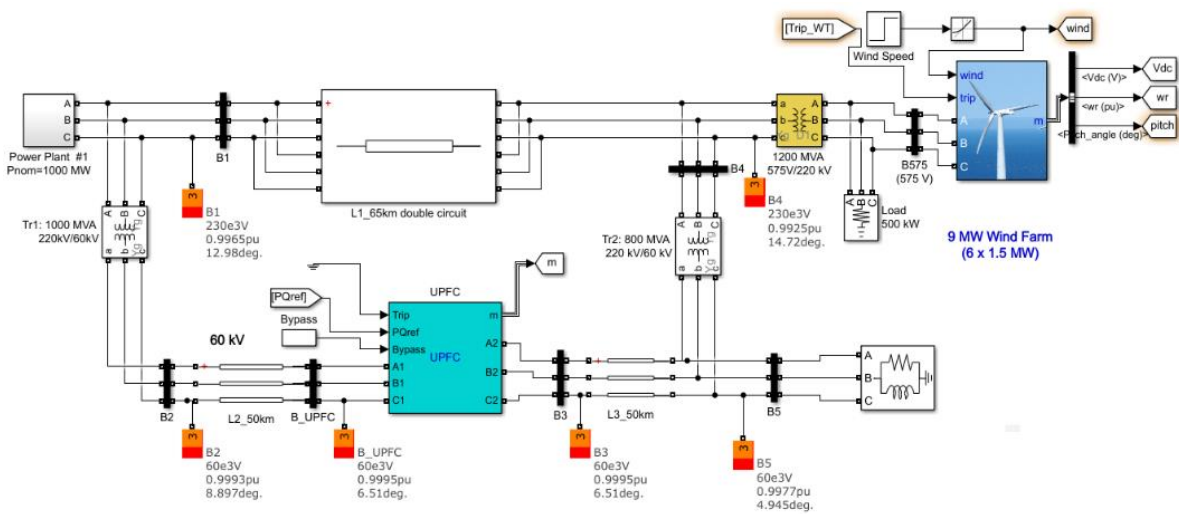


Figure 16. System connected to DFIG-based wind farm and UPFC

The plots of voltage magnitude (V_{pos}), the real power, and the reactive power (corresponding to each bus), obtained in simulations 3 and 4, are given in Figures 18 and 19, Figures 20 and 21, and Figures 22 and 23, respectively. These results confirm that the voltage values of the system have been improved using the UPFC. Furthermore, it is noticed that the characteristics of the load bus (5th bus) have been also improved. Specifically, the real power has increased from $P = 460.8 MW$ to $471.5 MW$ and the reactive power becomes $Q = 18.86 MVAR$.

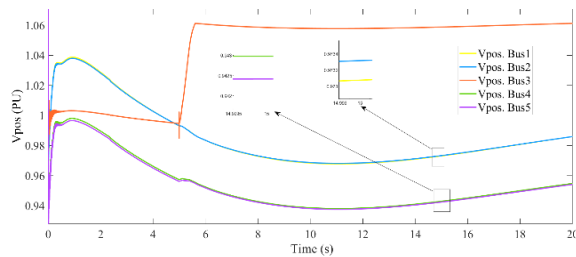


Figure 17. The curves of V_{pos} of each bus, obtained from simulation 3

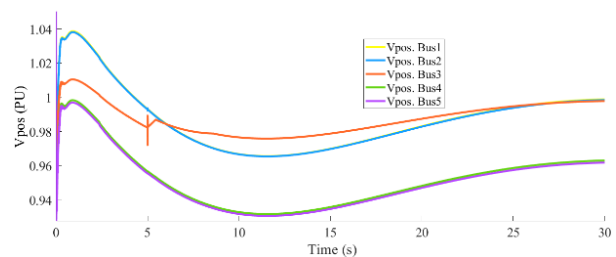


Figure 18. The V_{pos} curves of each bus, obtained from simulation 4

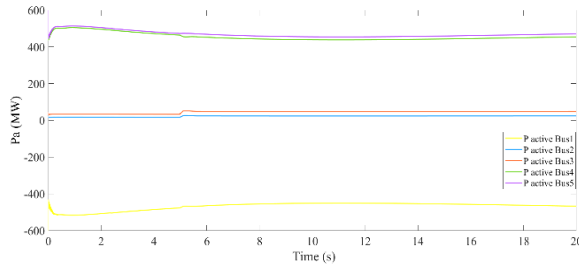


Figure 19. The active power curves obtained from simulation 3

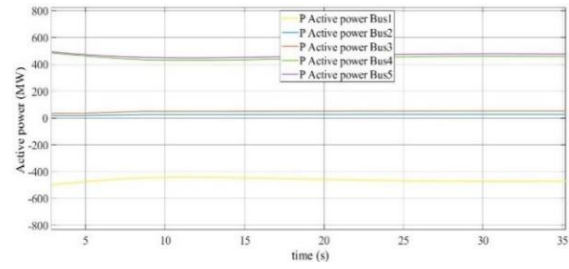


Figure 20. The active power curves obtained from simulation 4

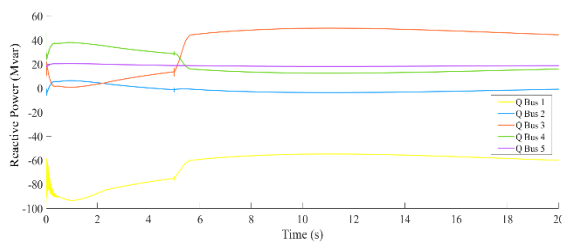


Figure 21. The curves of reactive powers obtained from simulation 3

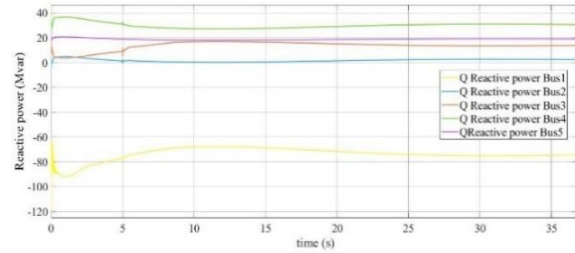


Figure 22. The curves of reactive powers obtained from simulation 4

The obtained results from simulations 3 and 4 corresponding to each bus are presented at Table 3 and Table 4. These results show that the voltage corresponding to buses 3, 4, and 5 has been improved, compared to those obtained above. For convenience, the grid parameter values (P , Q , and V_{pos}) obtained in the 5th bus are recapitulated in Table 5. The values of V_{pos} obtained in 3th and 4th buses are also given in Table 6. These results show that the best values are given using the UPFC controlled by a FLC (simulation 4).

Table 3. The obtained results from simulation 3 corresponding to each bus

Bus	B1	B2	B3	B4	B5
P (MW)	-467.5	24.49	48.46	455.2	471.5
Q(MVAR)	-58.93	-1.91	47.18	14.93	18.86
V(PU)	0.98	0.98	1.06	0.95	0.95
d(°)	12.98	8.897	6.51	14.72	4.946

Table 4. The obtained results from simulation 4 corresponding to each bus

Bus	B1	B2	B3	B4	B5
P (MW)	-469.2	28.46	51.92	458.9	474.7
Q(MVAR)	-51.86	-7.79	65.9	7.83	19
V(PU)	0.99	0.99	1.108	0.96	0.96
d(°)	12.98	8.897	6.51	14.72	4.946

Table 5. The grid parameter values (P , Q , and V_{pos}) in bus 5

Bus	V_{pos} (PU)		
	B5	B5	B5
1 st simulation	495.2	19.81	0.97
2 nd simulation	460.8	18.43	0.94
3 th simulation	471.5	18.86	0.95
4 th simulation	474.7	19	0.96

Table 6. The grid parameter values V_{pos} in bus 4 and bus3

Bus	V_{pos} (PU)	
	B4	B3
1 st simulation	0.98	0.98
2 nd simulation	0.94	0.96
3 th simulation	0.95	1.06
4 th simulation	0.96	1.108

5.2.1. The main conclusions of this results section

For convenience, the main conclusions of this results section are: Firstly, when there is no wind farm connected to the grid, the system does not present any perturbation. Secondly, when a wind farm is connected to the grid, the system performance has deteriorated. Thirdly, a UPFC is used to ameliorate the system’s performance. Then, the results show that the introduction of the UPFC improves the system’s performance. Finally, a FLC combined with the UPFC has been established. The obtained results show that the system performance has been significantly improved.

5.2.2. Sensitivity analysis

For convenience, the sensitivity analysis has been dealt. Then, in this sensitivity analysis, the following influencing parameters are chosen: the load active power (PA_{load}), the load reactive power (PR_{load}), the power wind farm (P_{wind}) and the position of the UPFC Di_{SUPFC} . The initial parameter values are $PA_{load}=500$ MW, $PR_{load}=20$ Mvar, $P_{wind}=9$ MW and $Di_{SUPFC}=50$ Km. The considered ranges of the parameters PA_{load} , PR_{load} , P_{wind} , and Di_{SUPFC} are $[0 - 100]$ (Km), $[0-550]$ (MW), $[0-22]$ (Mvar) and $[0-9.9]$ (MW), respectively. The results of this sensitivity analysis show that load active power is the most significant influencing parameter of the model.

6. CONCLUSION

This paper discusses the problem of the integration of wind turbines into the electrical grid. The wind turbines are based on DFIG machines. It is shown that the integration of the DFIG-based wind farm into the power system deteriorates the system performance. Especially, the power flow, the voltage drops, and the frequency response. To overcome these problems, the UPFC has been proposed. It is observed that the integration of the UPFC into the system improves its characteristics. To further improve the system characteristics, Fuzzy logic controllers have been used in the UPFC shunt and series regulators. The given results show that the system performances have been enhanced, especially the values of the active and reactive powers, and voltages in different buses. Accordingly, the implementation of the UPFC using the fuzzy logic controller is one of the best solutions to overcome the disturbances caused by the integration of DFIG-based wind farms into the electrical grid. The obtained numerical results show the effectiveness of this work. Furthermore, the problems caused by the wind farm integration to the grid are significantly reduced using the proposed FLC.

REFERENCES

- [1] M. E. Leirpoll, J. S. Næss, O. Cavalett, M. Dorber, X. Hu, and F. Cherubini, "Optimal combination of bioenergy and solar photovoltaic for renewable energy production on abandoned cropland," *Renewable Energy*, vol. 168, pp. 45–56, 2021, doi: 10.1016/j.renene.2020.11.159.
- [2] H. Solman, M. Smits, B. van Vliet, and S. Bush, "Co-production in the wind energy sector: A systematic literature review of public engagement beyond invited stakeholder participation," *Energy Research & Social Science*, vol. 72, 2020, p. 101876, 2021, doi: 10.1016/j.erss.2020.101876.
- [3] P. H. A. Barra, W. C. de Carvalho, T. S. Menezes, R. A. S. Fernandes, and D. V. Coury, "A review on wind power smoothing using high-power energy storage systems," *Renewable and Sustainable Energy Reviews*, vol. 137, p. 110455, 2021, doi: 10.1016/j.rser.2020.110455.
- [4] M. I. Mosaad, A. Alenany, and A. Abu-Siada, "Enhancing the performance of wind energy conversion systems using unified power flow controller," *IET Generation, Transmission & Distribution*, vol. 14, no. 10, pp. 1922–1929, 2020, doi: 10.1049/iet-gtd.2019.1112.
- [5] B. Wadawa, Y. Errami, A. Obbadi, and S. Sahnoun, "Robustification of the H_{∞} controller combined with fuzzy logic and PI&PID-Fd for hybrid control of Wind Energy Conversion System Connected to the Power Grid Based on DFIG," *Energy Reports*, vol. 7, pp. 7539–7571, 2021, doi: 10.1016/j.egyr.2021.10.120.
- [6] H. R. Shabani, M. Kalantar, and A. Hajizadeh, "Investigation of the closed-loop control system on the DFIG dynamic models in transient stability studies," *International Journal of Electrical Power & Energy Systems*, vol. 131, 2020, p. 107084, 2021, doi: 10.1016/j.ijepes.2021.107084.
- [7] S. Tamalouzi *et al.*, "Enhanced direct reactive power control-based multi-level inverter for dfig wind system under variable speeds," *Sustainability*, vol. 13, no. 16, 2021, doi: 10.3390/su13169060.
- [8] Y. Sahri *et al.*, "New intelligent direct power control of DFIG-based wind conversion system by using machine learning under variations of all operating and compensation modes," *Energy Reports*, vol. 7, pp. 6394–6412, 2021, doi: 10.1016/j.egyr.2021.09.075.
- [9] B. S. Goud, C. R. Reddy, M. Bajaj, E. E. Elattar, and S. Kamel, "Power quality improvement using distributed power flow controller with bwo-based fopid controller," *Sustainability*, vol. 13, no. 20, p. 11194, 2021, doi: 10.3390/su132011194.
- [10] A. A. Shehata, M. A. Tolba, A. M. El-Rifaie, and N. V. Korovkin, "Power system operation enhancement using a new hybrid methodology for optimal allocation of FACTS devices," *Energy Reports*, vol. 8, pp. 217–238, 2022, doi: 10.1016/j.egyr.2021.11.241.
- [11] A. Soroudi, "Controllable transmission networks under demand uncertainty with modular FACTS," *International Journal of Electrical Power & Energy Systems*, vol. 130, p. 106978, 2021, doi: 10.1016/j.ijepes.2021.106978.
- [12] B. B. Adetokun and C. M. Muriithi, "Application and control of flexible alternating current transmission system devices for voltage stability enhancement of renewable-integrated power grid: A comprehensive review," *Heliyon*, vol. 7, no. 3, p. e06461, 2021, doi: 10.1016/j.heliyon.2021.e06461.
- [13] B. Singh and R. Kumar, "A comprehensive survey on enhancement of system performances by using different types of FACTS controllers in power systems with static and realistic load models," *Energy Reports*, vol. 6, pp. 55–79, 2020, doi: 10.1016/j.egyr.2019.08.045.
- [14] S. Galvani, B. Mohammadi-Ivatloo, M. Nazari-Heris, and S. Rezaeian-Marjani, "Optimal allocation of static synchronous series compensator (SSSC) in wind-integrated power system considering predictability," *Electric Power Systems Research*, vol. 191, 2020, p. 106871, 2021, doi: 10.1016/j.epsr.2020.106871.
- [15] F. C. Neves, A. L. M. Coelho, and I. P. Faria, "A testbed for assessing the impact of static var compensator on loss of excitation protection of synchronous generators," *Electric Power Systems Research*, vol. 201, 2020, p. 107496, 2021, doi: 10.1016/j.epsr.2021.107496.

- [16] M. T. Hoq, J. Wang, and N. Taylor, "Review of recent developments in distance protection of series capacitor compensated lines," *Electric Power Systems Research*, vol. 190, 2020, p. 106831, 2021, doi: 10.1016/j.epsr.2020.106831.
- [17] J. H. Woo, L. Wu, S. M. Lee, J. -B. Park, and J. H. Roh, "D-STATCOM d-q axis current reference control applying DDPG algorithm in the distribution system," *IEEE Access*, vol. 9, pp. 145840–145851, 2021, doi: 10.1109/ACCESS.2021.3119745.
- [18] J. Ansari, A. R. Abbasi, M. H. Heydari, and Z. Avazzadeh, "Simultaneous design of fuzzy PSS and fuzzy STATCOM controllers for power system stability enhancement," *Alexandria Engineering Journal*, vol. 61, no. 4, pp. 2841–2850, 2022, doi: 10.1016/j.aej.2021.08.007.
- [19] A. Gupta, "Power quality evaluation of photovoltaic grid interfaced cascaded H-bridge nine-level multilevel inverter systems using D-STATCOM and UPQC," *Energy*, vol. 238, p. 121707, 2022, doi: 10.1016/j.energy.2021.121707.
- [20] H. Li, T. Zheng, S. Huang, and Y. Wang, "UPFC fault ride-through strategy based on virtual impedance and current limiting reactor," *International Journal of Electrical Power & Energy Systems*, vol. 125, 2020, p. 106491, 2021, doi: 10.1016/j.ijepes.2020.106491.
- [21] S. R. Paital, P. K. Ray, and S. R. Mohanty, "A robust dual interval type-2 fuzzy lead-lag based UPFC for stability enhancement using Harris Hawks Optimization," *ISA Transactions*, vol. 123, 2022, doi: 10.1016/j.isatra.2021.05.029.
- [22] J. Liu, Z. Xu, J. Yang, and Z. Zhang, "Modeling and Analysis for Global and Local Power Flow Operation Rules of UPFC Embedded System under Typical Operation Conditions," *IEEE Access*, vol. 8, pp. 21728–21741, 2020, doi: 10.1109/ACCESS.2020.2969500.
- [23] B. Rathore, O. P. Mahela, B. Khan, and S. Padmanaban, "Protection scheme using wavelet-alienation-neural technique for UPFC compensated transmission line," *IEEE Access*, vol. 9, pp. 13737–13753, 2021, doi: 10.1109/ACCESS.2021.3052315.
- [24] A. Hinda, M. Khat, and Z. Boudjema, "Advanced control scheme of a unified power flow controller using sliding mode control," *International Journal of Power Electronics and Drive System (IJPEDS)*, vol. 11, no. 2, pp. 625–633, 2020, doi: 10.11591/ijpeds.v11.i2.pp625-633.
- [25] K. M. Kotb, M. F. Elmorshedy, H. S. Salama, and A. Dán, "Enriching the stability of solar/wind DC microgrids using battery and superconducting magnetic energy storage based fuzzy logic control," *Journal of Energy Storage*, vol. 45, p. 103751, 2022, doi: 10.1016/j.est.2021.103751.
- [26] T. Yang, N. Sun, and Y. Fang, "Adaptive fuzzy control for uncertain mechatronic systems with state estimation and input nonlinearities," *IEEE Transactions on Industrial Informatics*, vol. 18, no. 3, pp. 1770–1780, 2022, doi: 10.1109/TII.2021.3089143.
- [27] S. Ghosh, "Neuro-fuzzy-based IoT assisted power monitoring system for smart grid," *IEEE Access*, vol. 9, pp. 168587–168599, 2021, doi: 10.1109/ACCESS.2021.3137812.
- [28] A. A. Salem, N. A. N. Aldin, A. M. Azmy, and W. S. E. Abdellatif, "Implementation and Validation of an Adaptive Fuzzy Logic Controller for MPPT of PMSG-Based Wind Turbines," *IEEE Access*, vol. 9, pp. 165690–165707, 2021, doi: 10.1109/access.2021.3134947.
- [29] L. Zhang, L. Zhang, J. Yang, M. Gao, and Y. Li, "Application research of fuzzy PID control optimized by genetic algorithm in medium and low speed Maglev train charger," *IEEE Access*, vol. 9, pp. 152131–152139, 2021, doi: 10.1109/ACCESS.2021.3123727.
- [30] G. Tahri, Z. A. Foitih, and A. Tahri, "Fuzzy logic control of active and reactive power for a grid-connected photovoltaic system using a three-level neutral-point-clamped inverter," *International Journal of Power Electronics and Drive System (IJPEDS)*, vol. 12, no. 1, pp. 453–462, 2021, doi: 10.11591/ijpeds.v12.i1.pp453-462.
- [31] P. Song, Z. Xu, H. Dong, H. Cai, and Z. Xie, "Security-constrained line loss minimization in distribution systems with high penetration of renewable energy using UPFC," *Journal of Modern Power Systems and Clean Energy*, vol. 5, no. 6, pp. 876–886, 2017, doi: 10.1007/s40565-017-0334-8.
- [32] Y. Muhammad, R. Akhtar, R. Khan, F. Ullah, M. A. Z. Raja, and J. A. T. Machado, "Design of fractional evolutionary processing for reactive power planning with FACTS devices," *Scientific Reports*, vol. 11, no. 593, 2021, doi: 10.1038/s41598-020-79838-2.
- [33] S. Kamel and F. Jurado, "Power flow analysis with easy modelling of interline power flow controller," *Electric Power Systems Research*, vol. 108, pp. 234–244, 2014, doi: 10.1016/j.epsr.2013.11.017.

BIOGRAPHIES OF AUTHORS



Tarik Rabyi    is currently completing his Ph.D. in integration of renewable energy in the grid under the supervision of Professor Adil Brouri, ENSAM (Higher National School of Arts and Trades), Moulay Ismail University, L2MC laboratory, SECNDCM team, Meknes Morocco. He received the Electrical engineer degree from ENSAM in 2002. He is conducting research activity on SRM, nonlinear control and identification, wind energy, and UPFC. He can be contacted at email: tarikensam@yahoo.fr.



Adil Brouri    In 2000, he obtained the Aggregation of Electrical Engineering and, in 2012, he obtained a Ph.D. in Automatic Control from the University of Mohammed 5, Morocco. He has been Professeur-Agrege for several years. Since 2013 he joined the ENSAM (Higher National School of Arts and Trades), My Ismail University in Meknes-Morocco. He obtained his HDR degree in 2015 at the ENSAM-Meknes (My Ismail University). His research interests include nonlinear system identification, nonlinear control, and SRM. He published several papers on the topics of identification of nonlinear system. Prof. Adil BROURI joined the research team "SECNDCM" and the L2MC (mechanical, mechatronics, and control) Laboratory as a permanent member. He can be contacted at email: a.brouri@ensam-umi.ac.ma.